

## Forecasting the Constraint on the Hu-Sawicki $f(R)$ Modified Gravity in the CSST $3 \times 2$ pt Photometric Survey

JUN-HUI YAN,<sup>1,2</sup> YAN GONG\*,<sup>1,2,3</sup> QI XIONG,<sup>1,2</sup> XUELEI CHEN,<sup>1,2,4,5,6</sup> QI GUO,<sup>7,8</sup> MING LI,<sup>7</sup> YUN LIU,<sup>7,8</sup> AND WENXIANG PEI<sup>9</sup>

<sup>1</sup>*National Astronomical Observatories, Chinese Academy of Sciences, Beijing 100101, China*

<sup>2</sup>*University of Chinese Academy of Sciences, Beijing 100049, China*

<sup>3</sup>*Science Center for China Space Station Telescope, National Astronomical Observatories, Chinese Academy of Sciences, 20A Datun Road, Beijing 100101, China*

<sup>4</sup>*Department of Physics, College of Sciences, Northeastern University, Shenyang 110819, China*

<sup>5</sup>*Centre for High Energy Physics, Peking University, Beijing 100871, China*

<sup>6</sup>*State Key Laboratory of Radio Astronomy and Technology, China*

<sup>7</sup>*National Astronomical Observatories, Chinese Academy of Sciences, 20A Datun Road, Beijing 100101, China*

<sup>8</sup>*School of Astronomy and Space Sciences, University of Chinese Academy of Sciences(UCAS), Yuquan Road NO.19A Beijing 100049, China*

<sup>9</sup>*Shanghai Key Lab for Astrophysics, Shanghai Normal University, Shanghai 200234, China*

### ABSTRACT

We forecast the constraint on the Hu-Sawicki  $f(R)$  model from the photometric survey operated by the Chinese Space Station Survey Telescope (CSST). The simulated  $3 \times 2$ pt data of galaxy clustering, weak lensing, and galaxy-galaxy lensing measurements within  $100 \text{ deg}^2$  are used in the analysis. The mock observational maps are constructed from a light cone, redshift sampling and noise. The angular power spectra are measured with pseudo- $C_\ell$  estimators and compared to theory in the same basis using validated weighting functions and an analytic covariance matrix that includes Gaussian, connected non-Gaussian, and super-sample terms. We model the theoretical spectra using two methods. The first one uses MGCAMB to compute the linear modified-gravity clustering power spectra, and the second one adopts the FREMU emulator with a baseline of nonlinear  $\Lambda$ CDM prescription. Parameter inference is performed with COBAYA, and the cosmological and modified-gravity parameters are sampled within the emulator training domain, which are jointly fitted with the systematic parameters. We find that the predictions from the two methods are in good agreement at the overlapping large scales, and the emulator method can correctly provide additional high- $\ell$  information. The  $1\sigma$  upper bounds of  $\log_{10} |f_{R0}|$  are found to be  $< -5.42$  for cosmic shear only case and  $< -5.29$  for the  $100 \text{ deg}^2$  CSST  $3 \times 2$ pt probe. The full CSST photometric survey with  $17,500 \text{ deg}^2$  survey area is expected to further improve the constraint precision by about one order of magnitude. Our results demonstrate that the CSST  $3 \times 2$ pt survey can deliver strict tests on  $f(R)$  gravity.

*Keywords:* Scalar-tensor-vector gravity (1428) – Large-scale structure of the universe (902) – Cosmological parameters(339)

### 1. INTRODUCTION

The discovery of late-time cosmic acceleration through observations of Type Ia supernovae (SNe Ia) (S. Perlmutter et al. 1999; A. G. Riess et al. 1998) has profoundly challenged our understanding of fundamental physics. The prevailing explanation invokes dark en-

ergy a component with negative pressure driving the accelerated expansion. The simplest realization is the cosmological constant  $\Lambda$  together with cold dark matter ( $\Lambda$ CDM) provides an excellent explanation to a broad suite of cosmological observations, including the anisotropies of cosmic microwave background (CMB) (e.g. N. Aghanim et al. 2020), cosmic large-scale structure (LSS) (e.g. S. Alam et al. 2021), and SN Ia distances (e.g. D. M. Scolnic et al. 2018).

Nonetheless, the cosmological constant raises significant theoretical puzzles, such as the fine-tuning and coincidence problems. Accordingly, another possibility is that the observed acceleration reflects a departure from Einstein’s general relativity (GR) on cosmological scales rather than the presence of a new exotic component. This leads to the idea of modified gravity theories, in which the law of gravity itself may differ at large scales, yielding accelerated expansion without invoking an additional dark energy fluid (T. Clifton et al. 2012).

Among modified gravity proposals,  $f(R)$  theories are one of the simplest and most extensively studied extensions (H. A. Buchdahl 1970; A. A. Starobinsky 1980). In these models, the Einstein-Hilbert action is generalized to include a function of the Ricci scalar  $R$ . As a concrete example, we consider the Hu-Sawicki parameterization of  $f(R)$  gravity (W. Hu & I. Sawicki 2007). This class of models introduces an additional scalar degree of freedom, which alters the relation between matter overdensities and metric potentials, and thereby modifies the growth history and power spectrum of large scale structure relative to GR.

Consequently, probes of structure formation including galaxy clustering, weak lensing, cluster abundances, and redshift-space distortions, provide direct and complementary tests of  $f(R)$  modifications. Current third-generation (Stage-III) surveys have already produced representative bounds on the Hu-Sawicki parameter, commonly expressed as upper limits on  $\log_{10}|f_{R0}|$ . Analyses of cosmic shear from KiDS-1000 suggest that when  $f_{R0}$  is included in nonlinear modeling, the data alone tend to yield weak, prior-dominated constraints (T. Tröster et al. 2021). Similarly, HSC-Y1 cosmic-shear studies which employ  $k$ -cut techniques to suppress small-scale modeling uncertainties report constraints that remain largely prior dominated (L. Vazsonyi et al. 2021).

Studies that combine weak lensing with other probes, e.g., cluster abundances with weak-lensing mass calibration, have achieved substantially stronger limits. For example, a recent joint analysis using SPT tSZE-selected clusters calibrated by Dark Energy Survey (DES) and Hubble Space Telescope (HST) weak lensing reports  $\log_{10}|f_{R0}| < -5.32$  (95% CL) (S. M. L. Vogt et al. 2025). More generally, combinations of Stage-III weak lensing (DES-Y3, KiDS-1000, HSC-Y3) with external datasets can push the upper bound on  $\log_{10}|f_{R0}|$  into the  $-4$  to  $-5$  range, with the precise limit sensitive to the choices in nonlinear modeling and screening implementation (J. Bai & J.-Q. Xia 2024).

In this work we focus on the  $3\times 2$ pt photometric observation of a forthcoming Stage-IV survey, i.e. the Chinese

Space Station Survey Telescope (CSST) (H. Zhan 2021; Y. Gong et al. 2019, 2025a,b). Our goal is to investigate the capability of constraining the Hu-Sawicki  $f(R)$  parameter with the CSST galaxy clustering and weak-lensing measurements alone (i.e., without CMB or other external probes), and evaluate CSST’s potential to distinguish modified gravity from the  $\Lambda$ CDM paradigm.

The structure of this paper is organized as follows. In Section 2, we introduce the theoretical framework of the Hu-Sawicki  $f(R)$  gravity model and derive the angular power spectrum formalism for the  $3\times 2$ pt analysis, including the treatment of systematic effects. Section 3 describes the construction of mock observational data from the CSST photometric survey, including galaxy clustering, cosmic shear, and galaxy-galaxy lensing measurements, along with the covariance matrix estimation. In Section 4, we present the parameter constraint methodology, and report the constraints on the Hu-Sawicki parameter  $\log_{10}|f_{R0}|$  and other cosmological parameters. Finally, Section 5 summarizes our main findings and discusses the potential of the full CSST survey for testing modified gravity theories.

## 2. THEORETICAL FRAMEWORK

### 2.1. The Hu-Sawicki Model of $f(R)$ Gravity

$f(R)$  theories extend the Einstein-Hilbert action by replacing the Ricci scalar  $R$  with a general function  $f(R)$ , thereby introducing an extra scalar degree of freedom that can mediate a long-range fifth force and requires screening mechanisms (e.g. the chameleon) to satisfy local gravity tests (W. Hu & I. Sawicki 2007; J. Khoury & A. Weltman 2004; A. De Felice & S. Tsujikawa 2010). The total action of  $f(R)$  gravity can be expressed as

$$S = \int d^4x \sqrt{-g} \left[ \frac{f(R)}{16\pi G} \right] + S_m + S_r, \quad (1)$$

where  $S_m$  and  $S_r$  denote the matter and radiation actions, respectively. Variation of Eq. (1) with respect to the metric yields the modified field equations:

$$f_R R_{\mu\nu} - \frac{1}{2} f g_{\mu\nu} - \nabla_\mu \nabla_\nu f_R + g_{\mu\nu} \square f_R = 8\pi G T_{\mu\nu}, \quad (2)$$

with  $f_R \equiv df/dR$  and  $\square \equiv g^{\alpha\beta} \nabla_\alpha \nabla_\beta$ .

Assuming a spatially flat FLRW metric, the Ricci scalar is  $R = 6(2H^2 + \dot{H})$ , where  $H \equiv \dot{a}/a$  and dots denote derivatives with respect to cosmic time  $t$ . The modified Friedmann equations become

$$3f_R H^2 = 8\pi G (\rho_m + \rho_r) + \frac{1}{2}(f_R R - f) - 3H \dot{f}_R, \quad (3)$$

$$-2f_R \dot{H} = 8\pi G (\rho_m + p_m + \rho_r + p_r) + \ddot{f}_R - H \dot{f}_R. \quad (4)$$

In the following analysis, we neglect the contributions from radiation ( $\rho_r$  and  $p_r$ ) as we focus on the late-time

universe. It is convenient to convert the geometric modifications into an effective energy density and pressure which are defined by

$$\rho_{\text{eff}} = \frac{1}{8\pi G} \left[ \frac{1}{2}(f_R R - f) - 3H \dot{f}_R + 3(1 - f_R)H^2 \right], \quad (5)$$

$$p_{\text{eff}} = \frac{1}{8\pi G} \times \left[ -\frac{1}{2}(f_R R - f) + \ddot{f}_R + 2H \dot{f}_R - (1 - f_R)(2\dot{H} + 3H^2) \right]. \quad (6)$$

With these definitions, the Friedmann equation can assume the familiar form  $3H^2 = 8\pi G(\rho_{\text{m}} + \rho_{\text{eff}})$ , and the effective equation of state is defined by  $w_{\text{eff}} \equiv p_{\text{eff}}/\rho_{\text{eff}}$  (T. P. Sotiriou & V. Faraoni 2010; A. De Felice & S. Tsujikawa 2010).

Under the quasi-static and sub-horizon approximation, i.e. neglecting time derivatives of perturbations relative to spatial derivatives, the linearized field equations in Newtonian gauge reduce to a modified Poisson equation and a scalaron (field) equation. Using the co-moving Laplacian  $\nabla^2$ , the following relations can be derived as (W. Hu & I. Sawicki 2007; A. De Felice & S. Tsujikawa 2010; J. Khoury & A. Weltman 2004)

$$\nabla^2 \Phi = \frac{16\pi G}{3} \delta\rho - \frac{1}{6} \delta R, \quad (7)$$

$$\nabla^2 \delta f_R = \frac{1}{3} (\delta R - 8\pi G \delta\rho), \quad (8)$$

where  $\delta f_R \equiv f_{RR} \delta R$  with  $f_{RR} \equiv d^2 f/dR^2$ , and  $\delta R$  and  $\delta\rho$  denote perturbations of the Ricci scalar and matter density.

W. Hu & I. Sawicki (2007) proposed an  $f(R)$  model that employs the chameleon mechanism to recover GR locally on high-density region, which can be parameterized as

$$f(R) = R - m^2 \frac{c_1 (R/m^2)^n}{c_2 (R/m^2)^n + 1}, \quad (9)$$

with  $m^2 \equiv 8\pi G \bar{\rho}_{\text{m}0}/3 = H_0^2 \Omega_{\text{m}0}$  and  $c_1, c_2$  and  $n$  are the dimensionless parameters. For  $R \gg m^2$  the expansion yields

$$f(R) \simeq R - \frac{c_1}{c_2} m^2 + \frac{c_1}{c_2^2} m^2 \left( \frac{m^2}{R} \right)^n, \quad (10)$$

so the background evolution can mimic  $\Lambda$ CDM with  $2\Lambda \simeq (c_1/c_2)m^2$  when the last term is negligible (W. Hu & I. Sawicki 2007).

The scalar degree of freedom  $f_R \equiv df/dR$  deviates slightly from unity in the large- $R$  limit, and the deviation can be written as

$$\tilde{f}_R \simeq 1 - n \frac{c_1}{c_2^2} \left( \frac{m^2}{R} \right)^{n+1}. \quad (11)$$

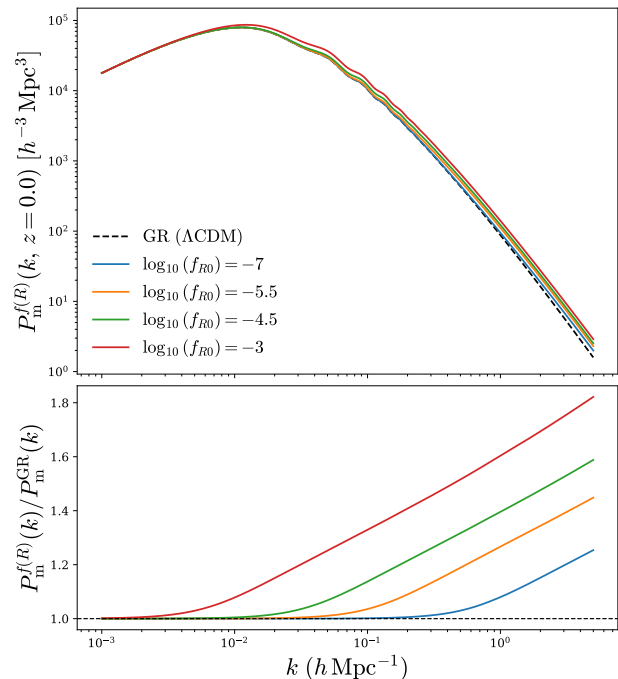


**Figure 1.** *Upper panel:* The linear matter power spectrum  $P_{\text{m}}(k)$  at  $z = 0$  for different values of  $\log_{10} |f_{R0}|$  and the  $\Lambda$ CDM model calculated by MGCAMB. *Lower panel:* The ratio  $P_{\text{m}}^{f(R)}(k)/P_{\text{m}}^{\Lambda\text{CDM}}(k)$  for different values of  $\log_{10} |f_{R0}|$ .

Here we fix  $n = 1$  to simplify the model and facilitate comparison with a wide range of existing studies. The present-day amplitude of this deviation can be defined by  $f_{R0} \equiv \tilde{f}_R(z = 0)$ . Small  $|f_{R0}|$  indicates close agreement with GR on cosmological scales. The influence of  $\log_{10} |f_{R0}|$  on the matter power spectrum at  $z = 0$  is presented in Figure 1, which shows a key observational feature of the enhanced power at small scales. As  $\log_{10} |f_{R0}|$  decreases, the chameleon screening mechanism becomes more efficient, suppressing this enhancement and causing the spectrum to approach the  $\Lambda$ CDM case. We can see that the deviation from the  $\Lambda$ CDM model becomes significant at  $k \gtrsim 0.002$  or  $0.2 h \text{ Mpc}^{-1}$  for  $\log_{10} |f_{R0}| = -3$  or  $-7$ .

## 2.2. Angular Power Spectrum

Accurate modeling of the observed angular power spectra requires careful treatment of several observational systematics that can bias cosmological inference. These include photometric redshift uncertainties, shear calibration, galaxy bias, and intrinsic alignments (IA) of galaxy shapes.

Photometric redshift uncertainties are modeled using the shift ( $\Delta_z^i$ ) and stretch ( $\sigma_z^i$ ) parameters for each tomographic bin  $i$ , which modify the estimated redshift

distributions as (Q. Xiong et al. 2025)

$$n^i(z) \rightarrow \frac{1}{\sigma_z^i} n^i \left( \frac{z - \langle z^i \rangle - \Delta_z^i}{\sigma_z^i} + \langle z^i \rangle \right). \quad (12)$$

Here, the superscript  $i$  denotes the redshift bin index, and  $\langle z^i \rangle \equiv \int z n^i(z) dz$  is the mean redshift of that bin. Shear calibration biases are included as the multiplicative factor  $(1 + m_i)$  for each tomographic bin. Intrinsic alignment effect arises from correlations with the large scale tidal field, introducing spurious signals in shear auto- and cross-correlations. We adopt the non-linear alignment (NLA) model (H. Hildebrandt et al. 2017; H. Johnston et al. 2019), in which the IA contribution for the  $i$ -th bin is given by

$$F^i(\chi) = -A_{\text{IA}} C_1 \rho_c \frac{\Omega_m}{D(\chi)} n^i(z(\chi)) \frac{dz}{d\chi} \left( \frac{1+z}{1+z_0} \right)^{\eta_{\text{IA}}}, \quad (13)$$

where  $A_{\text{IA}}$  and  $\eta_{\text{IA}}$  are the free parameters,  $C_1 = 5 \times 10^{-14} h^{-2} M_\odot^{-1} \text{Mpc}^3$ ,  $\rho_c$  is the present critical density,  $D(\chi)$  is the linear growth factor, and  $z_0 = 0.6$  is the pivot redshift.

Once all relevant effects are modeled, the theoretical angular power spectra are computed under the Limber approximation (D. N. Limber 1953; M. LoVerde & N. Afshordi 2008), which provides an accurate description on small and intermediate angular scales. For a generic field  $X$  and  $Y$ , the cross spectrum between tomographic bins  $i$  and  $j$  is

$$C_{XY}^{ij}(\ell) = \int_0^{\chi_{\text{max}}} \frac{d\chi}{\chi^2} W_X^i(\chi) W_Y^j(\chi) P_m \left( \frac{\ell + 1/2}{\chi}, z(\chi) \right), \quad (14)$$

where  $W_X^i(\chi)$  and  $W_Y^j(\chi)$  are the weighting functions of the two probes. The weighting functions for shear ( $\kappa$ ), galaxy clustering ( $g$ ), and IA are

$$W_\kappa^i(\chi) = \frac{3H_0^2 \Omega_m}{2c^2} \frac{\chi}{a(\chi)} \int_\chi^{\chi_{\text{max}}} d\chi' n^i(z(\chi')) \frac{dz}{d\chi'} \frac{\chi' - \chi}{\chi'}, \quad (15)$$

$$W_g^i(\chi) = b^i n^i(z(\chi)) \frac{dz}{d\chi}, \quad (16)$$

$$W_{\text{IA}}^i(\chi) = F^i(\chi). \quad (17)$$

The full  $3 \times 2$ pt vector combines the auto- and cross-correlations of galaxy clustering ( $gg$ ), cosmic shear ( $\kappa\kappa$ ), and galaxy-galaxy lensing ( $g\kappa$ ). The observed angular power spectra are given by (D. Huterer et al. 2006; T. M. C. Abbott et al. 2018)

$$\tilde{C}_{gg}^{ij}(\ell) = C_{gg}^{ij}(\ell) + \delta_{ij} \frac{1}{\bar{n}_g^i}, \quad (18)$$

$$\tilde{C}_{\kappa\kappa}^{ij}(\ell) = (1 + m_i)(1 + m_j) \left[ C_{\kappa\kappa}^{ij}(\ell) + C_{\text{II}}^{ij}(\ell) + C_{\text{GI}}^{ij}(\ell) \right] + \delta_{ij} \frac{\sigma_\gamma^2}{\bar{n}_g^i}, \quad (19)$$

$$\tilde{C}_{g\kappa}^{ai}(\ell) = (1 + m_i) \left[ C_{g\kappa}^{ai}(\ell) + C_{g\text{I}}^{ai}(\ell) \right]. \quad (20)$$

Here,  $\delta_{ij}$  is the Kronecker delta, which ensures shot noise and shape noise contributes only to auto-correlations within the same tomographic bin,  $\bar{n}_g^i$  denotes the mean galaxy number density in the  $i$ -th bin, and  $\sigma_\gamma$  represents the per-component intrinsic ellipticity dispersion of source galaxies, characterizing shape noise in weak-lensing measurements. These noise and calibration terms are included to ensure unbiased recovery of the cosmological power spectra.

### 3. MOCK DATA

To assess the constraining power of CSST on Hu-Sawicki  $f(R)$  gravity, we construct high-fidelity mock catalogs and maps tailored to the CSST photometric survey using the Jiutian simulations (J. Han et al. 2025; Q. Xiong et al. 2025). These mocks are derived from a large-volume  $N$ -body simulation with  $6144^3$  dark matter particles in a  $1 h^{-1} \text{Gpc}$  box, adopting a fiducial cosmology consistent with Planck 2018 results (N. Aghanim et al. 2020). With a particle mass of approximately  $3.72 \times 10^8 h^{-1} M_\odot$ , the simulation captures the nonlinear structure formation essential for our analysis. The mock footprint covers approximately  $100 \text{deg}^2$ , matching the scope of the present study.

In the simulation, dark matter evolves within a cubic volume of order  $(\text{Gpc } h^{-1})^3$ . Halos and subhalos are identified with Friends-of-Friends and SUBFIND, tracing the cosmic web across time (V. Springel et al. 2001; V. Springel 2005). A semi-analytic galaxy population model, calibrated to deep multi-band observations, populates halos to match the CSST depth and bandpasses (B. M. B. Henriques et al. 2015; W. Pei et al. 2024). Each galaxy is assigned a photometric redshift with a scatter of  $\sigma_z = 0.05(1+z)$ . The sample is divided into four tomographic bins spanning  $z \in [0, 3]$  to extract more information. The resulting effective source density is  $\bar{n}_{\text{eff}} \simeq 26 \text{arcmin}^{-2}$ . The resulting galaxy redshift distribution and weighting functions for the galaxy clustering and weak lensing kernels are shown in Figure 2.

The weak lensing maps are produced with multi-plane ray tracing along the light-cone, yielding shear and convergence fields matched to the matter distribution. Galaxy clustering maps are obtained by projecting the

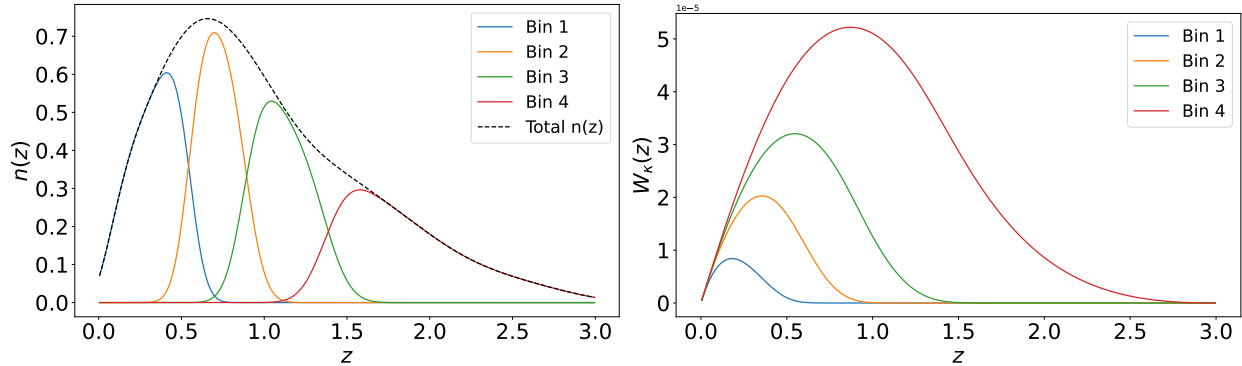


**Figure 2.** *Left panel:* Galaxy redshift distributions  $n(z)$  for the four tomographic bins (colored curves), with the normalized total distribution shown as the black dashed line. *Right panel:* The corresponding lensing weight functions  $W_\kappa(z)$  for each bin used in the cosmic shear analysis.

three-dimensional overdensity in each tomographic slice onto the sky (Z. Chen & Y. Yu 2024). These products yield realistic  $\kappa\kappa$ ,  $gg$ , and  $g\kappa$  signals suited to a full  $3 \times 2$ pt analysis.

The maps are rendered on uniform Cartesian grids with angular resolution sufficient for  $\ell_{\max} \approx 3000$ . The noise realizations follow the CSST characteristics and are derived based on the results from current observations. We adopt the per-component variance  $\sigma_\gamma^2 = 0.04$  for the shape noise in the shear maps and the Poisson shot noise is added to the galaxy clustering maps in each redshift bin. Our noise realizations are uncorrelated between tomographic bins, and shot noise contributes only to auto-correlations.

We estimate the angular power spectra  $C_\ell$  for all auto- and cross-correlations on flat-sky patches using Fourier estimators, with logarithmically spaced multipole bins over  $\ell \in [50, 3000]$  to balance large-scale sensitivity and small-scale modeling. Mode coupling from masks is handled through pseudo- $C_\ell$  deconvolution (P. Peebles 2012; E. Hivon et al. 2002; G. Chon et al. 2004; C. Hikage et al. 2010).

The joint covariance of the  $3 \times 2$ pt data vector is decomposed into three components: Gaussian, connected non-Gaussian (cNG) (T. Hamana et al. 2004; M. Takada & B. Jain 2004; D. Huterer et al. 2006), and super-sample covariance (SSC) (W. Hu & B. Jain 2004; M. Takada & W. Hu 2013). Following the methodology validated in Q. Xiong et al. (2025), we have  $\text{Cov} = \text{Cov}^{\text{Gauss}} + \text{Cov}^{\text{cNG}} + \text{Cov}^{\text{SSC}}$ . The Gaussian term is computed analytically as the four-point contraction of two power spectra, which is given by

$$\begin{aligned} \text{Cov}_{ij,kl;XY,X'Y'}^{\text{Gauss}}(\ell, \ell') &= \frac{\delta_{\ell\ell'}^{\text{K}}}{(2\ell + 1)f_{\text{sky}}\Delta\ell} \\ &\times \left[ \tilde{C}_{XX'}^{ik}(\ell) \tilde{C}_{YY'}^{jl}(\ell) + \tilde{C}_{XY'}^{il}(\ell) \tilde{C}_{YX'}^{jk}(\ell) \right], \end{aligned} \quad (21)$$

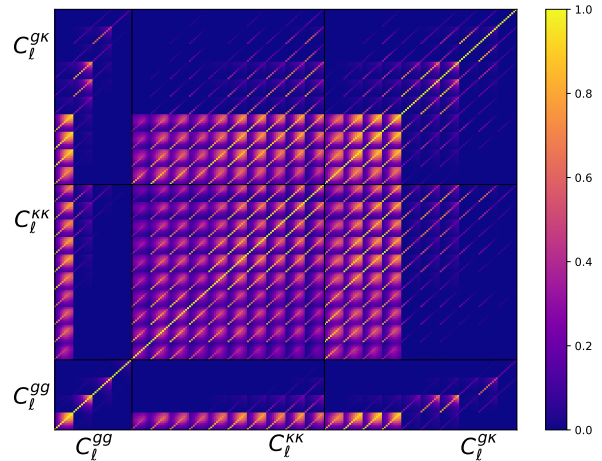


**Figure 3.** The normalized covariance matrix for the joint  $3 \times 2$ pt data vector, structured by tomographic bin and probe type ( $gg$ ,  $\kappa\kappa$ ,  $g\kappa$ ). The matrix shows the correlation coefficients between all measured angular power spectrum combinations.

where  $X, X', Y, Y' \in \{g, \kappa\}$  denote the tracer types (galaxy or convergence),  $i, j, k, l$  index the tomographic bins,  $f_{\text{sky}}$  is the survey sky fraction, and  $\Delta\ell$  is the multipole bin width. For non-Gaussian terms, the cNG term captures mode coupling arising from nonlinear structure formation and becomes increasingly important at high multipoles, and the SSC term quantifies the coupling between modes within the survey and long-wavelength background density fluctuations. The non-Gaussian covariance components are computed using the CCL code (N. E. Chisari et al. 2019; L. D. C. C. Library 2019), and the normalized covariance matrix is shown in Figure 3.

In Figures 4, 5, and 6, we show the observed galaxy, shear, and galaxy-galaxy lensing angular power spectra, respectively. The  $1\sigma$  error bars are from the diagonal of the covariance matrix. The theoretical curves from two parallel pipelines are also shown, i.e. a lin-

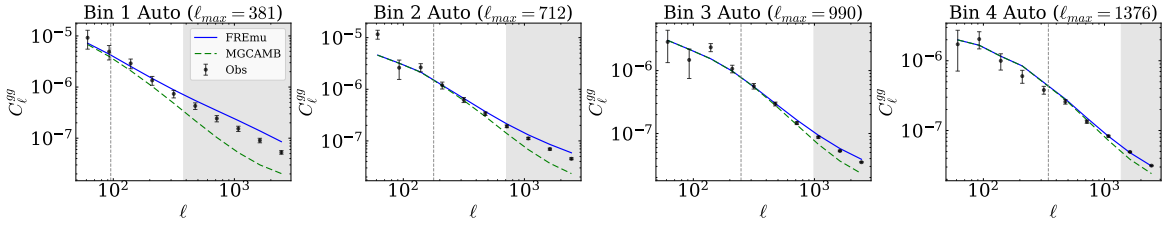


**Figure 4.** The simulated angular power spectra  $C_{gg}^{ij}(\ell)$  of the CSST galaxy clustering survey for the four tomographic bins. The solid blue and dashed green curves show the prediction using FREMU and MGCAMB at  $\log_{10}|f_{R0}| = -6$ , respectively. The error bars are derived from the diagonal of the covariance matrix. The gray region indicates the multipoles excluded by the scale cut at  $k = 0.4 h \text{Mpc}^{-1}$ . The vertical gray dashed lines mark  $\ell_{\text{max}}$  corresponding to  $k = 0.1 h \text{Mpc}^{-1}$ .

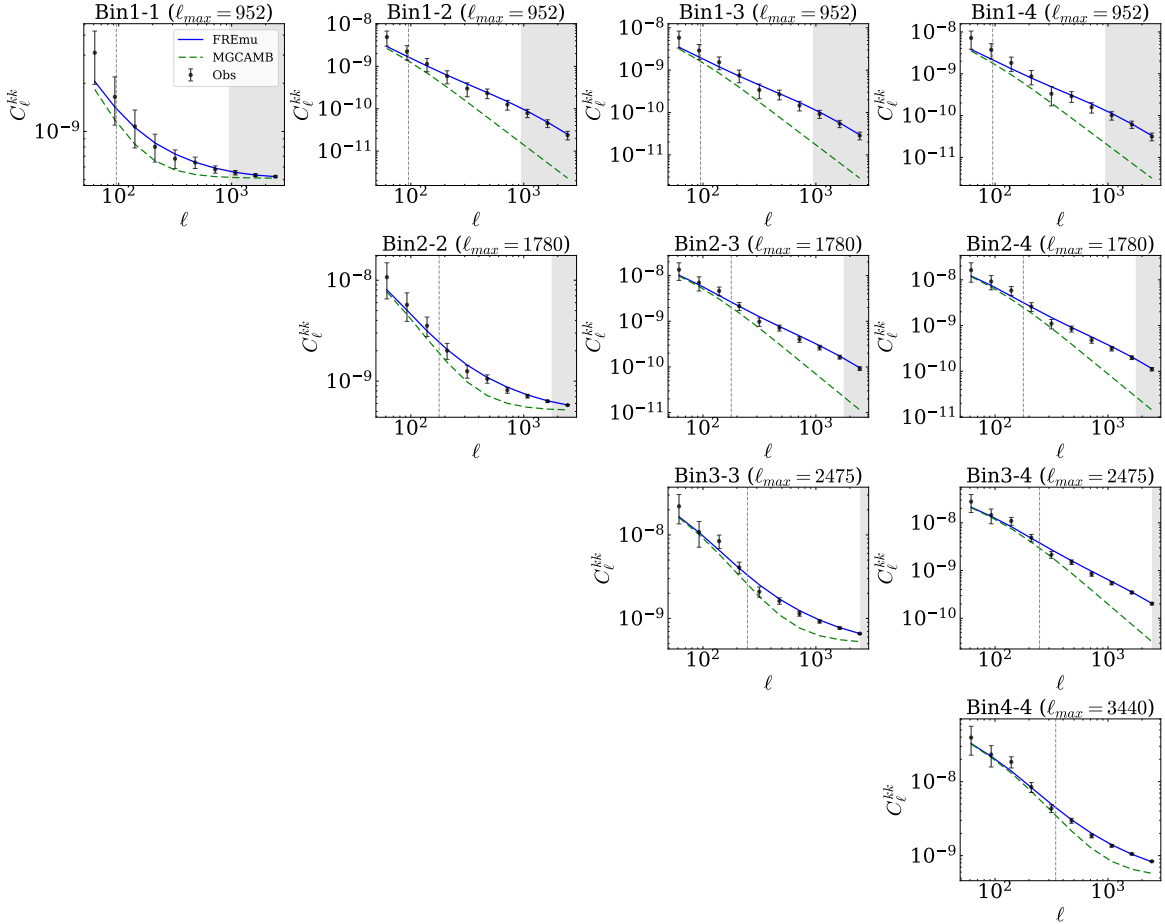


**Figure 5.** The simulated angular power spectra  $C_{\kappa\kappa}^{ij}(\ell)$  of the CSST shear measurement for the four tomographic bins. The solid blue and dashed green curves show the prediction using FREMU and MGCAMB at  $\log_{10}|f_{R0}| = -6$ , respectively. The error bars are derived from the diagonal of the covariance matrix. The gray region indicates the multipoles excluded by the scale cut at  $k = 1.0 h \text{Mpc}^{-1}$ . The vertical gray dashed lines mark  $\ell_{\text{max}}$  corresponding to  $k = 0.1 h \text{Mpc}^{-1}$ .

ear theory pipeline using MGCAMB (A. Lewis et al. 2000; G.-B. Zhao et al. 2009; A. Zucca et al. 2019; A. Hojjati et al. 2011; Z. Wang et al. 2023), and a non-linear pipeline using the FREMU emulator (J. Bai & J.-Q. Xia 2024; J. Bai et al. 2025). To control modeling systematics, we impose  $k$ -space cuts and map them to per-bin multipole cuts via  $\ell_{\text{max}}^{(i)} = k_{\text{max}} \chi(\langle z^{(i)} \rangle)$ . In the linear pipeline, we adopt  $k_{\text{max}} = 0.1, h, \text{Mpc}^{-1}$  for all

probes, which corresponds to the vertical gray dashed lines in Figures 4, 5, and 6. In the emulator pipeline, we use  $k_{\text{max}} = 0.4 h \text{Mpc}^{-1}$  for  $gg$  and  $g\kappa$  to limit the impact of small scale uncertainties such as nonlinear screening residuals and potential baryonic effects, and set  $k_{\text{max}} = 1.0 h \text{Mpc}^{-1}$  for  $\kappa\kappa$ , which is determined by the FREMU training upper bound. The gray shaded

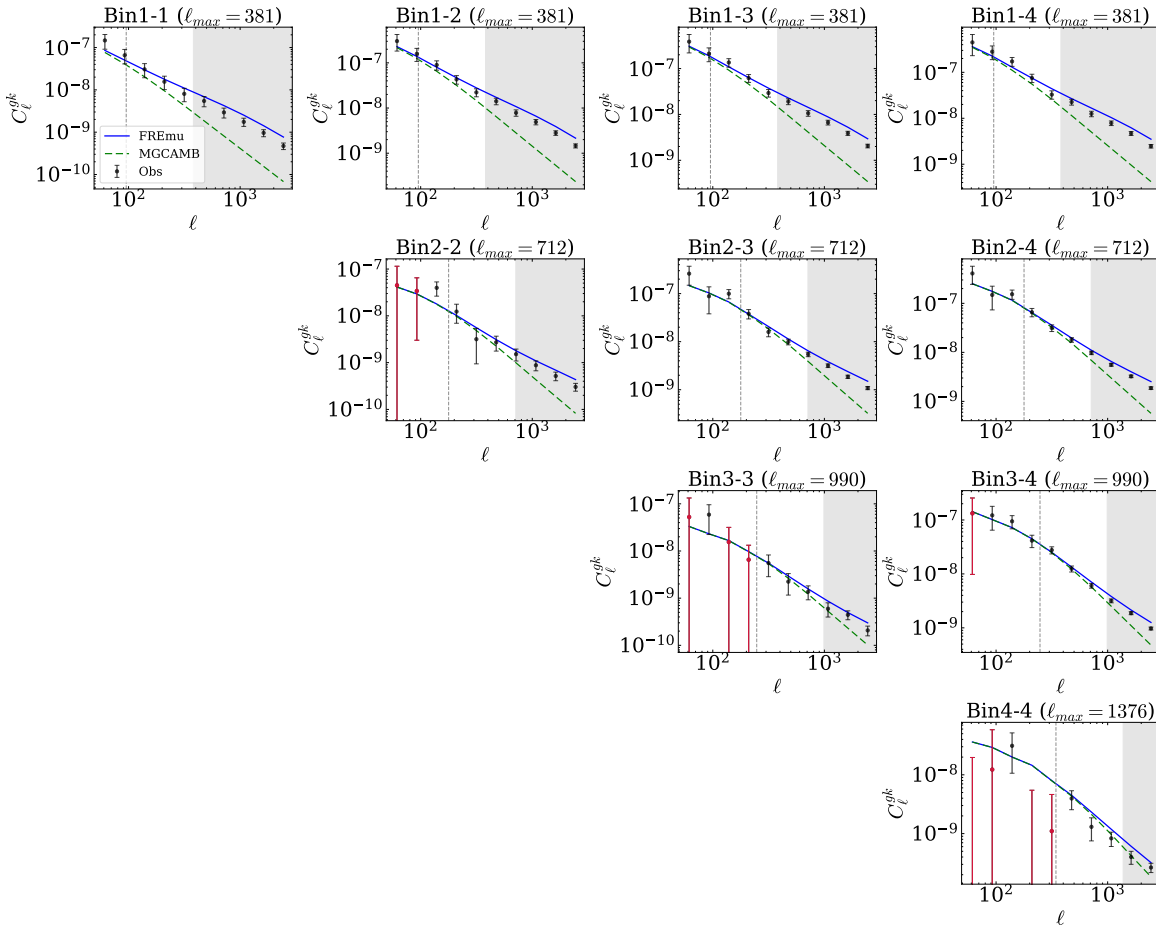


**Figure 6.** The simulated angular power spectra  $C_{g\kappa}^{ij}(\ell)$  of the CSST galaxy-galaxy lensing measurement for the four tomographic bins. The solid blue and dashed green curves show the prediction using FREMU and MGCAMB at  $\log_{10}|f_{R0}| = -6$ , respectively. The error bars are derived from the diagonal of the covariance matrix. The gray region indicates the multipoles excluded by the scale cut at  $k = 0.4 h \text{ Mpc}^{-1}$ . The vertical gray dashed lines mark  $\ell_{\text{max}}$  corresponding to  $k = 0.1 h \text{ Mpc}^{-1}$ . Data points with signal-to-noise ratio (SNR) below unity are highlighted in red to indicate low statistical significance.

regions in Figures 4, 5, and 6 indicate the multipoles excluded by the applicable cuts.

## 4. PARAMETER CONSTRAINTS

### 4.1. Constraint Process

We employ a Bayesian framework to infer the posterior distributions of the cosmological, modified gravity, and systematic parameters from the measured angular power spectra, using Markov chain Monte Carlo (MCMC) sampling. To structure the analysis, we define data vectors  $\vec{D}_X = \tilde{C}_X^{ij}(\ell)$ , where  $X \in gg, \kappa\kappa, g\kappa$ , which concatenate all tomographic bin pairs and multipoles for each probe. The log-likelihood for each probe is assumed to be Gaussian and is given by

$$\ln \mathcal{L}_X = -\frac{1}{2}(\vec{D}_X - \vec{T}_X(\theta))^T \mathbf{C}_X^{-1}(\vec{D}_X - \vec{T}_X(\theta)), \quad (22)$$

where  $\vec{T}_X(\theta)$  are the theoretical angular power spectra considering the systematic terms, and  $\mathbf{C}_X$  are the cor-

responding covariances including the Gaussian and non-Gaussian terms (cNG and SSC), with the Gaussian part given by Eq. (21).

The posterior follows Bayes' theorem with priors specified in Table 1. The priors of the cosmological parameters and modified gravity amplitude we adopt are fully contained within the FREMU training hypercube, ensuring emulator validity across the sampled parameter space. We vary the intrinsic alignment amplitude  $A_{IA}$  and its redshift evolution  $\eta_{IA}$ , acknowledging that the present setup has limited constraining power on  $\eta_{IA}$ . For this mock-based study we disable explicit modeling of baryonic feedback, since the mocks do not include baryonic physics and our scale selection reduces baryonic sensitivity.

As mentioned, we consider two routes to compute the theoretical angular power spectra that enter the likelihood. The first route uses MGCAMB, which solves the linearized Boltzmann-Einstein equations in

**Table 1.** The free parameters considered in our constraint process. The first column shows the names of the free parameters, and the second and third columns show the fiducial values and the priors of the parameters, respectively. Uniform priors are described by  $\mathcal{U}(x, y)$ , with  $x$  and  $y$  denoting the prior range. The Gaussian priors are represented by  $\mathcal{N}(\mu, \sigma)$ , where  $\mu$  and  $\sigma$  are the mean and standard deviation, respectively.

Parameter	Fiducial Value	Prior
<b>Cosmology</b>		
$H_0$	67.66	$\mathcal{U}(50, 90)$
$\Omega_m$	0.3111	$\mathcal{U}(0.1, 0.5)$
$\Omega_b$	0.0490	$\mathcal{U}(0.03, 0.07)$
$\log(10^{10} A_s)$	3.05	$\mathcal{U}(1.61, 3.91)$
$n_s$	0.9665	$\mathcal{U}(0.8, 1.2)$
$\log_{10}  f_{R0} $	-	$\mathcal{U}(-7.0, -3.5)$
<b>Intrinsic alignment</b>		
$A_{IA}$	0	$\mathcal{U}(-5, 5)$
$\eta_{IA}$	0	$\mathcal{U}(-5, 5)$
<b>Galaxy bias</b>		
$b_g^i$	-	$\mathcal{U}(0, 5)$
<b>Photo-z shift</b>		
$\Delta z^i$	(0, 0, 0, 0)	$\mathcal{N}(0, 0.01)$
<b>Photo-z stretch</b>		
$\sigma_z^i$	(1, 1, 1, 1)	$\mathcal{N}(1, 0.05)$
<b>Shear calibration</b>		
$m_i$	(0, 0, 0, 0)	$\mathcal{N}(0, 0.01)$

the Hu-Sawicki model, yields the linear matter power spectrum, and provides modified growth and lensing responses at the perturbative level. We then project the resulting spectra to obtain  $C_\ell$  for  $gg$ ,  $\kappa\kappa$ , and  $g\kappa$  under the same tomographic windows used in the measurements. Since a validated nonlinear prescription for modified gravity is not included in this setup, we restrict to  $k_{\max} = 0.1 h \text{ Mpc}^{-1}$  for all probes, as indicated by the gray dashed lines in Figures 4-6. This route serves as a conservative reference that isolates information from the linear regime.

The second route employs the emulator FREMU, which returns the ratio  $B(k, z) \equiv P_{f(R)}(k, z)/P_{\Lambda\text{CDM}}(k, z)$  over a validated training domain in parameter space, redshift, and wavenumber. We obtain a nonlinear prediction for  $f(R)$  by multiplying  $B(k, z)$  with a baseline nonlinear prescription for  $\Lambda\text{CDM}$ . This construction preserves the large scale agreement with the linear route and extends to smaller scales under controlled modeling. We have verified that the results of the two routes are in good agreement on the overlapping large-scale range, as shown

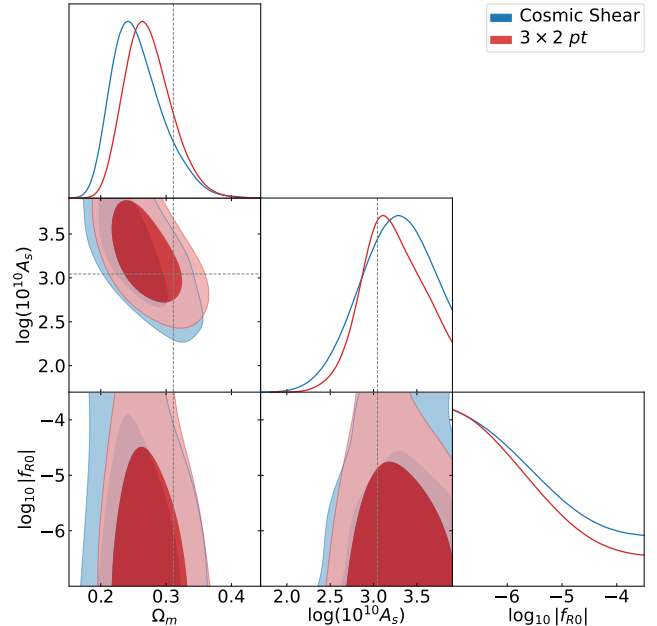


**Figure 7.** The contour maps (68% and 95% CLs) and 1D PDFs of  $\Omega_m$ ,  $\log(10^{10} A_s)$ ,  $\log_{10} |f_{R0}|$  for the CSST shear and  $3 \times 2pt$  measurements in  $100 \text{ deg}^2$  from the FREMU emulator. The dashed lines indicate the fiducial values of the parameters.

in Figures 4-6, while the emulator can correctly retain additional high  $\ell$  information.

For parameter inference, we use COBAYA (J. Torrado & A. Lewis 2021, 2019) to run MCMC sampling. We implement probe specific likelihoods for  $gg$ ,  $\kappa\kappa$ , and  $g\kappa$  under both routes. We assess the convergence of our Markov chains using the Gelman-Rubin statistic quantity  $R$ . Chains are considered converged when  $R - 1 < 0.01$ . To minimize the influence of the initial sampling phase, we discard the first 30% of each chain as burn-in and use the remaining samples for posterior inference.

#### 4.2. Constraint Results

Our analysis reveals a stark contrast in constraining power between the two theoretical approaches. The MGCAMB-based linear analysis fails to provide a meaningful constraint on  $\log_{10} |f_{R0}|$ , as the Hu-Sawicki model's deviations from GR are subtle on the linear scales ( $k_{\max} = 0.1 h \text{ Mpc}^{-1}$ ) accessible to this method and are dwarfed by statistical uncertainties. In contrast, the FREMU emulator, by incorporating nonlinear information, enables a significant detection of the modified gravity signal.

The resulting constraints from the FREMU-based analysis are summarized in Figure 7. For the cosmic shear-only ( $\kappa\kappa$ ) case, we find  $\log_{10} |f_{R0}| < -5.29$

( $-3.83$ ) at the 68% (95%) confidence level. The joint  $3 \times 2$ pt analysis tightens this constraint to  $\log_{10} |f_{R0}| < -5.42$  ( $-3.88$ ). Beyond the modified gravity parameter, the joint analysis also improves the precision on the standard  $\Lambda$ CDM cosmology: the relative uncertainty on  $\Omega_m$  improves from 15.4% to 13.0%, and on  $\log(10^{10} A_s)$  from 11.8% to 10.3%.

It is worth noting that the 100 deg<sup>2</sup> dataset provides relatively weak constraints on other cosmological parameters such as  $H_0$ ,  $\Omega_b$ , and  $n_s$ , as shown in the full posterior distributions in the Appendix. This is reasonable given the limited sky coverage and the inherent degeneracies in the current  $3 \times 2$ pt data vector.

The constraining power is expected to increase dramatically with the full CSST photometric survey covering 17,500 deg<sup>2</sup>. The enhanced measurement precision on large-scale modes will be particularly beneficial for galaxy clustering, and the constraint on  $\log_{10} |f_{R0}|$  could be improved by approximately an order of magnitude in this case. Furthermore, the full survey will also provide significantly improved constraints on parameters like  $H_0$ ,  $\Omega_b$ , and  $n_s$  through better measurement of the large-scale angular power spectra. This positions the full CSST survey to deliver exceptionally stringent tests of the Hu-Sawicki model and to break degeneracies in the full cosmological parameter space.

These results demonstrate that the CSST  $3 \times 2$ pt analysis can achieve competitive constraints using its internal data alone. This capability is noteworthy, as current Stage-III surveys often find that cosmic shear alone yields prior-dominated constraints on  $f(R)$  gravity, frequently requiring combination with external datasets like CMB and BAO to achieve stringent bounds (L. Vazsonyi et al. 2021; J. Bai et al. 2025; S. M. L. Vogt et al. 2025).

## 5. SUMMARY

In this work, we have established a robust analysis framework to assess the potential of the CSST  $3 \times 2$ pt photometric survey for constraining the Hu Sawicki  $f(R)$  gravity model. Our approach integrates high fidelity mock observations that capture the essential features of the survey, including photometric redshift sampling, shape and shot noise, and mask induced mode coupling. We measured the angular power spectra for galaxy clustering, cosmic shear, and galaxy galaxy lensing from these mocks. For theoretical predictions, we employed two complementary methods: a linear theory approach using MGCAMB restricted to conservative scales of  $k_{\max} = 0.1, h, \text{Mpc}^{-1}$ , and a nonlinear approach utilizing the FREMU emulator, which extends to  $k_{\max} = 0.4, h, \text{Mpc}^{-1}$  for galaxy clustering and galaxy

galaxy lensing, and  $k_{\max} = 1.0, h, \text{Mpc}^{-1}$  for cosmic shear. The two methods show good agreement on overlapping large scales, with the emulator successfully incorporating additional information from smaller scales.

We performed parameter inference with the MCMC sampler in COBAYA, using probe specific likelihoods and a block diagonal covariance approximation. The cosmological and modified gravity parameters were sampled within the validated domain of the FREMU emulator, while simultaneously marginalizing over a comprehensive set of systematic parameters, including those for intrinsic alignment, photometric redshift uncertainties, galaxy bias, and shear calibration. Our analysis shows that the CSST  $3 \times 2$ pt 100 deg<sup>2</sup> survey delivers constraints on  $\log_{10} |f_{R0}|$  that are competitive with, and in fact slightly tighter than, those from current Stage III surveys.

The constraining power is projected to improve substantially with the full CSST photometric survey covering 17,500 deg<sup>2</sup>. Future analyses combining this dataset with external probes such as CMB lensing and cluster abundances are expected to enable exceptionally stringent tests of modified gravity models and possible deviations from General Relativity on cosmological scales.

## ACKNOWLEDGMENTS

J.H.Y and Y.G. acknowledge the support from the CAS Project for Young Scientists in Basic Research (No. YSBR-092), and National Key R&D Program of China grant Nos. 2022YFF0503404 and 2020SKA0110402. X.L.C. acknowledges the support of the National Natural Science Foundation of China through grant Nos. 11473044 and 11973047 and the Chinese Academy of Science grants ZDKYYQ20200008, QYZDJ-SSW-SLH017, XDB 23040100, and XDA15020200. Q.G. acknowledges the support from the National Natural Science Foundation of China (NSFC No. 12033008). The Jiutian simulations were conducted under the support of the science research grants from the China Manned Space Project with grant No. CMS-CSST-2021-A03. This work is also supported by science research grants from the China Manned Space Project with grant Nos. CMS-CSST-2025-A02, CMS-CSST-2021-B01, and CMS-CSST-2021-A01.

*Software:* COBAYA (J. Torrado & A. Lewis 2021, 2019), MGCAMB (A. Lewis et al. 2000; G.-B. Zhao et al. 2009; A. Zucca et al. 2019; A. Hojjati et al. 2011; Z. Wang et al. 2023), CCL (N. E. Chisari et al. 2019; L. D. C. C. Library 2019), FREMU (J. Bai & J.-Q. Xia 2024; J. Bai et al. 2025), GETDIST (A. Lewis 2025)

## APPENDIX

In this appendix we present the full posterior constraints for all cosmological parameters (Figure 8) and systematic parameters (Figure 9), under the FREMU emulator method. Unless otherwise stated, the chains adopt the scale selection described in the main text (with  $gg$  and  $g\kappa$  restricted to  $k_{\max} = 0.4 h \text{ Mpc}^{-1}$  and  $\kappa\kappa$  to  $k_{\max} = 1.0 h \text{ Mpc}^{-1}$ ). We show the constraint results for the cosmic shear only ( $\kappa\kappa$ ) and the joint  $3 \times 2$ pt combination ( $gg$ ,  $g\kappa$ ,  $\kappa\kappa$ ) cases. These figures complement the focused three-parameter result shown in Figure 7, and provide a complete picture of systematic and cosmological degeneracies under the adopted likelihood and covariance matrix.

## REFERENCES

- Abbott, T. M. C., Abdalla, F. B., Alarcon, A., et al. 2018, *Phys. Rev. D*, 98, 043526, doi: [10.1103/PhysRevD.98.043526](https://doi.org/10.1103/PhysRevD.98.043526)
- Aghanim, N., et al. 2020, *Astron. Astrophys.*, 641, A6, doi: [10.1051/0004-6361/201833910](https://doi.org/10.1051/0004-6361/201833910)
- Alam, S., et al. 2021, *Phys. Rev. D*, 103, 083533, doi: [10.1103/PhysRevD.103.083533](https://doi.org/10.1103/PhysRevD.103.083533)
- Bai, J., & Xia, J.-Q. 2024, *Mon. Not. R. Astron. Soc.*, 528, 1234, doi: [10.1093/mnras/stae001](https://doi.org/10.1093/mnras/stae001)
- Bai, J., Xia, J.-Q., & Zhao, G.-B. 2025, *Astrophys. J.*, 992, 205, doi: [10.3847/1538-4357/ae07c4](https://doi.org/10.3847/1538-4357/ae07c4)
- Buchdahl, H. A. 1970, *Mon. Not. R. Astron. Soc.*, 150, 1, doi: [10.1093/mnras/150.1.1](https://doi.org/10.1093/mnras/150.1.1)
- Chen, Z., & Yu, Y. 2024, *Mon. Not. Roy. Astron. Soc.*, 534, 1205, doi: [10.1093/mnras/stae2150](https://doi.org/10.1093/mnras/stae2150)
- Chisari, N. E., Alonso, D., Krause, E., et al. 2019, *The Astrophysical Journal Supplement Series*, 242, 2, doi: [10.3847/1538-4365/ab1658](https://doi.org/10.3847/1538-4365/ab1658)
- Chon, G., Challinor, A., Prunet, S., Hivon, E., & Szapudi, I. 2004, *Monthly Notices of the Royal Astronomical Society*, 350, 914, doi: [10.1111/j.1365-2966.2004.07737.x](https://doi.org/10.1111/j.1365-2966.2004.07737.x)
- Clifton, T., Ferreira, P. G., Padilla, A., & Skordis, C. 2012, *Physics Reports*, 513, 1, doi: [10.1016/j.physrep.2012.01.001](https://doi.org/10.1016/j.physrep.2012.01.001)
- De Felice, A., & Tsujikawa, S. 2010, *Living Reviews in Relativity*, 13, 3, doi: [10.12942/lrr-2010-3](https://doi.org/10.12942/lrr-2010-3)
- Gong, Y., Liu, X., Cao, Y., et al. 2019, *Astrophys. J.*, 883, 203, doi: [10.3847/1538-4357/ab391e](https://doi.org/10.3847/1538-4357/ab391e)
- Gong, Y., et al. 2025a, <https://arxiv.org/abs/2507.04618>
- Gong, Y., et al. 2025b, *Sci. China Phys. Mech. Astron.*, 68, 280402, doi: [10.1007/s11433-025-2646-2](https://doi.org/10.1007/s11433-025-2646-2)
- Hamana, T., Takada, M., & Yoshida, N. 2004, *Mon. Not. Roy. Astron. Soc.*, 350, 893, doi: [10.1111/j.1365-2966.2004.07691.x](https://doi.org/10.1111/j.1365-2966.2004.07691.x)
- Han, J., et al. 2025, *Sci. China Phys. Mech. Astron.*, 68, 109511, doi: [10.1007/s11433-025-2712-1](https://doi.org/10.1007/s11433-025-2712-1)
- Henriques, B. M. B., White, S., Thomas, P., et al. 2015, *Mon. Not. Roy. Astron. Soc.*, 451, 2663, doi: [10.1093/mnras/stv705](https://doi.org/10.1093/mnras/stv705)
- Hikage, C., Takada, M., Hamana, T., & Spergel, D. 2010, *Monthly Notices of the Royal Astronomical Society*, 412, 65–74, doi: [10.1111/j.1365-2966.2010.17886.x](https://doi.org/10.1111/j.1365-2966.2010.17886.x)
- Hildebrandt, H., et al. 2017, *Mon. Not. Roy. Astron. Soc.*, 465, 1454, doi: [10.1093/mnras/stw2805](https://doi.org/10.1093/mnras/stw2805)
- Hivon, E., Górski, K. M., Netterfield, C. B., et al. 2002, *The Astrophysical Journal*, 567, 2, doi: [10.1086/338126](https://doi.org/10.1086/338126)
- Hojjati, A., Pogosian, L., & Zhao, G.-B. 2011, *Journal of Cosmology and Astroparticle Physics*, 2011, 005–005, doi: [10.1088/1475-7516/2011/08/005](https://doi.org/10.1088/1475-7516/2011/08/005)
- Hu, W., & Jain, B. 2004, *Phys. Rev. D*, 70, 043009, doi: [10.1103/PhysRevD.70.043009](https://doi.org/10.1103/PhysRevD.70.043009)
- Hu, W., & Sawicki, I. 2007, *Phys. Rev. D*, 76, 064004, doi: [10.1103/PhysRevD.76.064004](https://doi.org/10.1103/PhysRevD.76.064004)
- Huterer, D., Takada, M., Bernstein, G., & Jain, B. 2006, *Mon. Not. Roy. Astron. Soc.*, 366, 101, doi: [10.1111/j.1365-2966.2005.09782.x](https://doi.org/10.1111/j.1365-2966.2005.09782.x)
- Johnston, H., Georgiou, C., Joachimi, B., et al. 2019, *Astronomy & Astrophysics*, 624, A30, doi: [10.1051/0004-6361/201834714](https://doi.org/10.1051/0004-6361/201834714)
- Khoury, J., & Weltman, A. 2004, *Phys. Rev. D*, 69, 044026, doi: [10.1103/PhysRevD.69.044026](https://doi.org/10.1103/PhysRevD.69.044026)
- Lewis, A. 2025, *JCAP*, 08, 025, doi: [10.1088/1475-7516/2025/08/025](https://doi.org/10.1088/1475-7516/2025/08/025)
- Lewis, A., Challinor, A., & Lasenby, A. 2000, *The Astrophysical Journal*, 538, 473–476, doi: [10.1086/309179](https://doi.org/10.1086/309179)
- Library, L. D. C. C. 2019,, <https://github.com/LSSTDESC/CCL>
- Limber, D. N. 1953, *Astrophys. J.*, 117, 134, doi: [10.1086/145672](https://doi.org/10.1086/145672)
- LoVerde, M., & Afshordi, N. 2008, *Physical Review D*, 78, doi: [10.1103/physrevd.78.123506](https://doi.org/10.1103/physrevd.78.123506)
- Peebles, P. 2012, *Annual Review of Astronomy and Astrophysics*, 50, 1, doi: <https://doi.org/10.1146/annurev-astro-081811-125526>

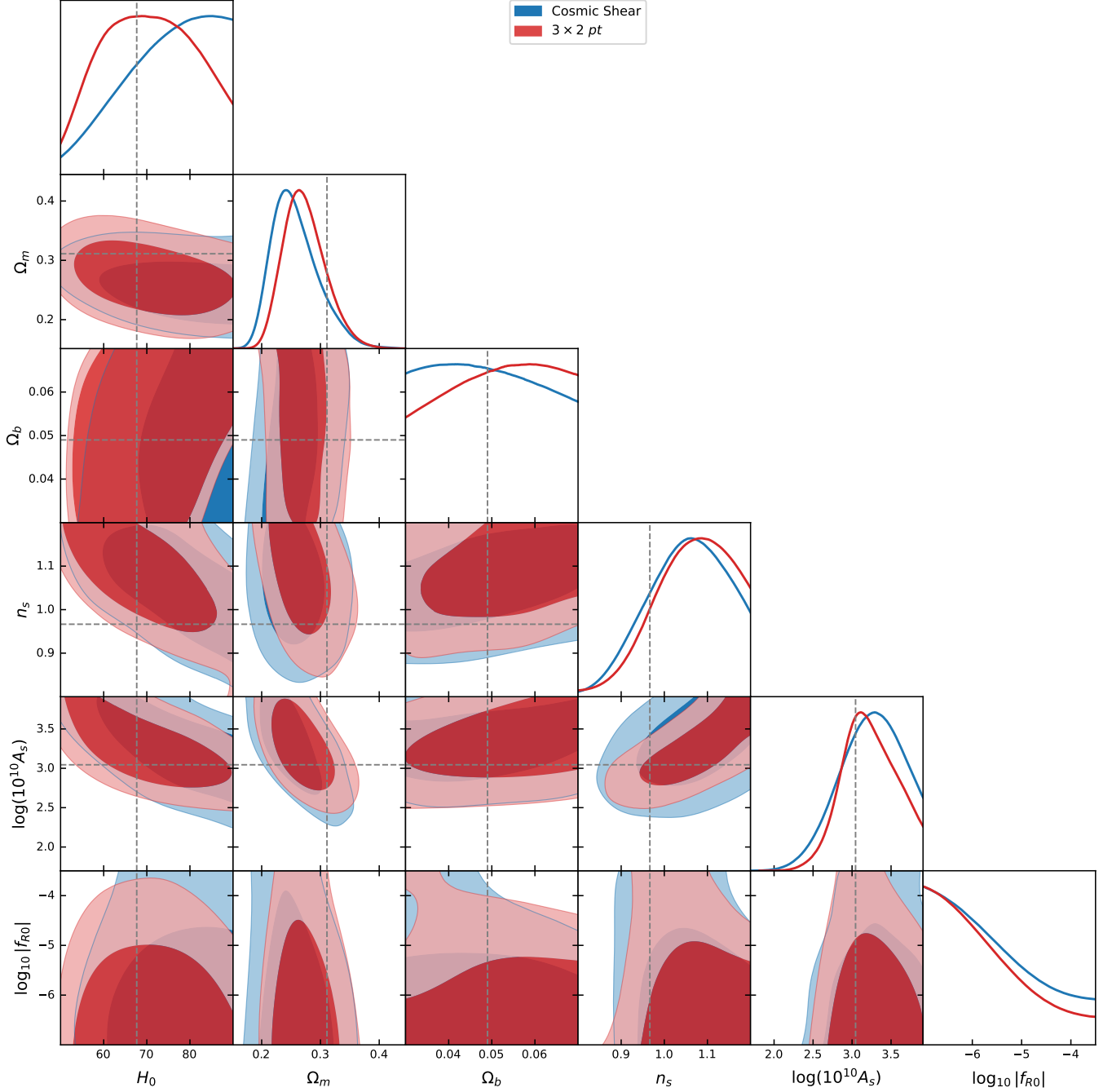


**Figure 8.** The contour maps (68% and 95% CLs) and 1D PDFs of all cosmological parameters considered in this work for the CSST shear and  $3 \times 2pt$  measurements in  $100 \text{ deg}^2$  from the FREMU emulator. The dashed lines indicate the fiducial values of the parameters.

Pei, W., Guo, Q., Li, M., et al. 2024,  
<https://arxiv.org/abs/2404.00092>

Perlmutter, S., et al. 1999, *Astrophys. J.*, 517, 565,  
 doi: [10.1086/307221](https://doi.org/10.1086/307221)

Riess, A. G., et al. 1998, *Astron. J.*, 116, 1009,  
 doi: [10.1086/300499](https://doi.org/10.1086/300499)

Scolnic, D. M., et al. 2018, *Astrophys. J.*, 859, 101,  
 doi: [10.3847/1538-4357/aab9bb](https://doi.org/10.3847/1538-4357/aab9bb)

Sotiriou, T. P., & Faraoni, V. 2010, *Reviews of Modern Physics*, 82, 451, doi: [10.1103/RevModPhys.82.451](https://doi.org/10.1103/RevModPhys.82.451)

Springel, V. 2005, *Mon. Not. Roy. Astron. Soc.*, 364, 1105,  
 doi: [10.1111/j.1365-2966.2005.09655.x](https://doi.org/10.1111/j.1365-2966.2005.09655.x)

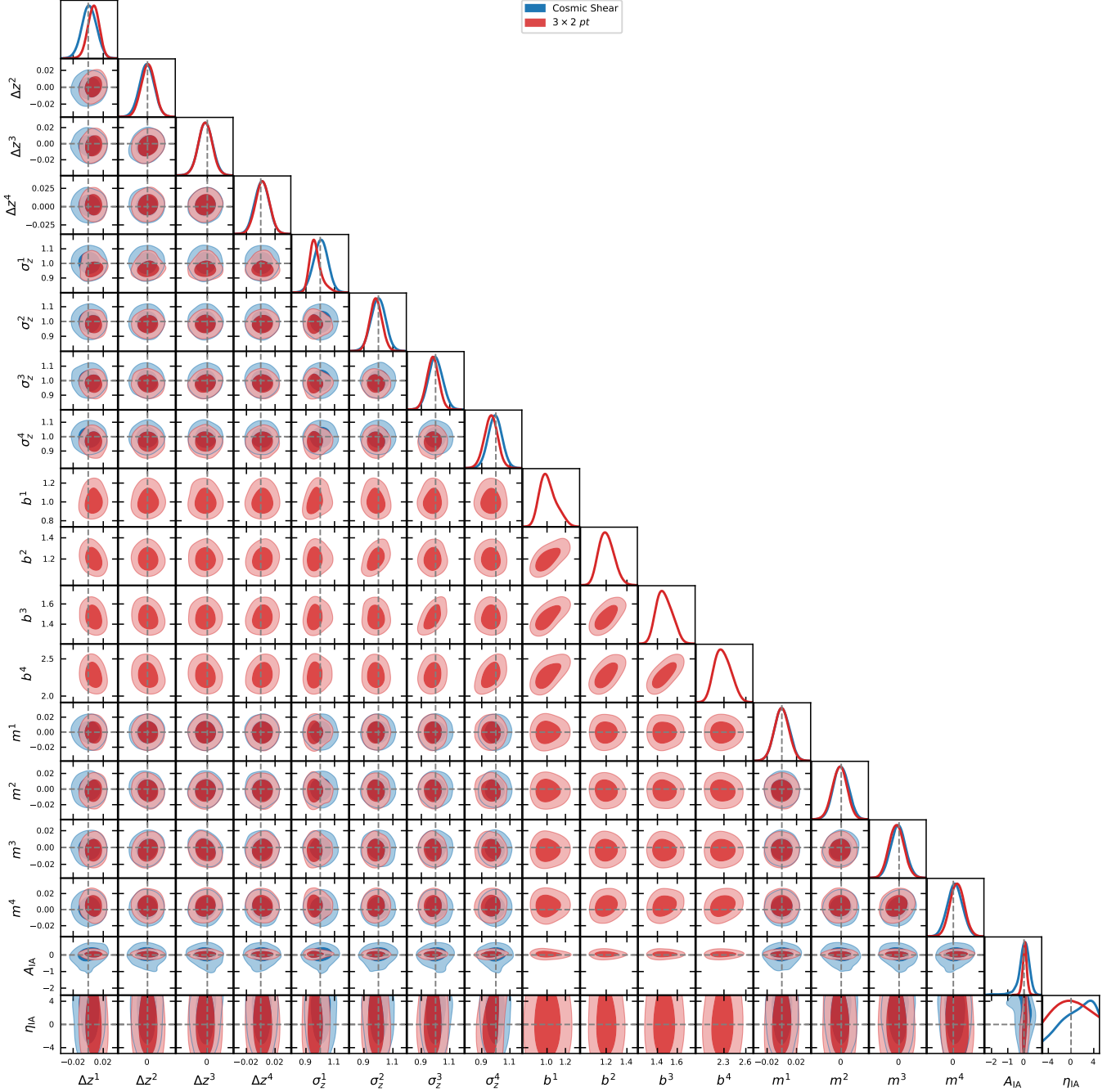


**Figure 9.** The contour maps (68% and 95% CLs) and 1D PDFs of the systematic parameters for the intrinsic alignment ( $A_{IA}$ ,  $\eta_{IA}$ ), photo- $z$  shift  $\Delta z^i$  and stretch  $\sigma_z^i$ , galaxy bias  $b_g^i$ , and shear calibration  $m_i$  for the CSST shear and  $3 \times 2$ pt measurements in  $100 \text{ deg}^2$  from the FREMU emulator. The dashed lines indicate the fiducial values of the parameters.

Springel, V., Yoshida, N., & White, S. D. M. 2001, *New Astron.*, 6, 79, doi: [10.1016/S1384-1076\(01\)00042-2](https://doi.org/10.1016/S1384-1076(01)00042-2)

Starobinsky, A. A. 1980, *Phys. Lett. B*, 91, 99, doi: [10.1016/0370-2693\(80\)90670-X](https://doi.org/10.1016/0370-2693(80)90670-X)

Takada, M., & Hu, W. 2013, *Phys. Rev. D*, 87, 123504, doi: [10.1103/PhysRevD.87.123504](https://doi.org/10.1103/PhysRevD.87.123504)

Takada, M., & Jain, B. 2004, *Mon. Not. Roy. Astron. Soc.*, 348, 897, doi: [10.1111/j.1365-2966.2004.07410.x](https://doi.org/10.1111/j.1365-2966.2004.07410.x)

Torrado, J., & Lewis, A. 2019, *Astrophysics Source Code Library*. <http://ascl.net/1910.019>

Torrado, J., & Lewis, A. 2021, *Journal of Cosmology and Astroparticle Physics*, 2021, 057, doi: [10.1088/1475-7516/2021/05/057](https://doi.org/10.1088/1475-7516/2021/05/057)

- Tröster, T., Asgari, M., Blake, C., et al. 2021, *Astron. Astrophys.*, 649, A88, doi: [10.1051/0004-6361/202039805](https://doi.org/10.1051/0004-6361/202039805)
- Vazsonyi, L., Taylor, P. L., Valogiannis, G., et al. 2021, *Phys. Rev. D*, 104, 083527, doi: [10.1103/PhysRevD.104.083527](https://doi.org/10.1103/PhysRevD.104.083527)
- Vogt, S. M. L., et al. 2025, *Phys. Rev. D*, 111, 043519, doi: [10.1103/PhysRevD.111.043519](https://doi.org/10.1103/PhysRevD.111.043519)
- Wang, Z., Mirpoorian, S. H., Pogolian, L., Silvestri, A., & Zhao, G.-B. 2023, *Journal of Cosmology and Astroparticle Physics*, 2023, 038, doi: [10.1088/1475-7516/2023/08/038](https://doi.org/10.1088/1475-7516/2023/08/038)
- Xiong, Q., et al. 2025, *Astrophys. J.*, 985, 131, doi: [10.3847/1538-4357/adcb44](https://doi.org/10.3847/1538-4357/adcb44)
- Zhan, H. 2021, *Chinese Science Bulletin*, 66, 1290, doi: [10.1360/TB-2021-0016](https://doi.org/10.1360/TB-2021-0016)
- Zhao, G.-B., Pogolian, L., Silvestri, A., & Zylberberg, J. 2009, *Physical Review D*, 79, doi: [10.1103/physrevd.79.083513](https://doi.org/10.1103/physrevd.79.083513)
- Zucca, A., Pogolian, L., Silvestri, A., & Zhao, G. 2019, *Journal of Cosmology and Astroparticle Physics*, 2019, 001–001, doi: [10.1088/1475-7516/2019/05/001](https://doi.org/10.1088/1475-7516/2019/05/001)